Noname manuscript No.
(will be inserted by the editor)

A novel gait generation method independent of target settling-time adjustment for underactuated limit cycle walking

Fumihiko Asano

Received: date / Accepted: date

Abstract This paper proposes a novel gait generation method for surely achieving constraint on impact posture in limit cycle walking. First, we introduce an underactuated rimless wheel model without ankle-joint actuation, and formulate a state-space realization of the control output using the stance-leg angle as a time parameter through an input-output linearization. Second, we determine a control input that moves the control output to a terminal value at a target stance-leg angle during the single-support phase. Third, we conduct numerical simulations to observe the fundamental gait properties, and discuss the relationship between the gait symmetry and mechanical energy restoration. Furthermore, we mathematically prove the asymptotic stability of the generated walking gait by analytically deriving the restored mechanical energy.

Keywords Limit cycle walking · Stability · Hybrid zero dynamics · Symmetry · Gait generation

1 Introduction

One of the physical characteristics of limit-cycle walkers including passive-dynamic walkers [1–9] is one-degree-of-underactuation at ankles. This implies that they walk actively but without explicitly considering the condition of the zero moment point (ZMP) [10]. Such underactuated dynamic walkers can generate a stable waking gait by achieving constraint on impact posture; they control the relative joint angles except the ankles to the steady terminal values

F. Asano
School of Information Science, Japan Advanced Institute of Science and Technology
1-1 Asahidai, Nomi, Ishikawa 923-1292, Japan
Tel.: +81-761-51-1243
Fax: +81-761-51-1149
E-mail: fasano@jaist.ac.jp

by the next impact and fall down as a 1-DOF rigid body in the same position. It was shown that the stability of the generated gait with constraint on impact posture is equivalent to that of the hybrid zero dynamics (HZD) or the discrete behavior of the stance-leg's angular velocity [4,8,9].

It has been considered difficult to determine the stability and efficiencies of limit cycle walking without conducting numerical simulations due to the complexity of a hybrid dynamical system. Theoretically, a sustainable walking gait can be generated by achieving the following three conditions unless with an unusual setting of the system parameters.

(C1) The walker completes an output-following control of the relative joint angles except those of the ankles to the steady terminal ones by the next impact to fall down as a 1-DOF rigid body in the same position (constraint on impact posture [4,8,9]).
(C2) The walker has sufficient kinetic energy or momentum to overcome the potential barrier at mid-stance.
(C3) The condition of unilateral constraint is always satisfied or the ground reaction force is always kept positive during motion.

The condition (C1) is the most important to guarantee the stability of a limit-cycle with state jumps and to make the gait analysis easy. If the walking system satisfies all the three conditions, then the gait stability can be determined as a one-dimensional return map of the angular velocity of the stance leg from immediately before or immediately after impact to the next [4,8,9]. For achieving (C1), however, the control parameter must be suitably chosen by trial and error in general. The most important parameter among others is the target settling-time and we must adjust it so that the output-following control can be completed during the single-support (stance) phases or by the next impact [8,9].

Based on the observations, in this paper we propose a novel method for surely achieving the constraint on impact posture by focusing on the property that the stance-leg angle monotonically increases during the single-support phases in limit cycle walking. First, we introduce a model of an underactuated rimless wheel (URW) [8,9] that consists of a rimless wheel (RW) [1,3,9] and a torso for analysis and develop the mathematical model. Second, we choose the relative joint angle between the RW and torso as the control output, and develop a state-space realization for it through an input-output linearization by using the stance-leg angle as a time parameter. The linearized system formulated is controllable, and the control input for settling the control output to the terminal value at a target stance-leg angle can be easily determined by using a controllability grammian. Third, we discuss how the gait properties change according to the target stance-leg angle or the symmetry of the generated trajectory through numerical simulations, and mathematically prove that the HZD of a sufficiently asymmetric gait is always asymptotically stable by analytically deriving the restored mechanical energy. Throughout this paper, we report two significant results on limit cycle walking. One is the importance of the gait asymmetry in mechanical energy restoration, and the other is that

the two conditions, constraints on impact posture and restored mechanical energy, are simultaneously achievable for the simplest underactuated limit cycle walker with a constant inertia matrix.

The subsequent sections are organized as follows. Section 2 describes the mathematical model of the URW. Section 3 considers an input-output linearization by using the stance-leg angle as a time parameter and develops the control law for surely achieving the constraint on impact posture. Section 4 analyzes the gait efficiencies through numerical simulations and gives a proof of the asymptotic stability of the generated walking gait. Finally, Section 5 concludes this paper and describes the future research direction.

2 Model of underactuated rimless wheel

2.1 Equation of motion

The URW model shown in Figure 1 consists of an eight-legged symmetrically-shaped RW and a torso link [8,9]. The torso link is connected to the RW at the central position, and the URW can exert a joint torque, u, between the torso and RW. The inertia moment of the torso about the CoM (center of mass) is I [kg·m^2], and the masses of the RW and torso are m_1 and m_2 [kg], respectively. It is assumed without loss of generality that the leg frames are massless. This condition is just for deriving the simplest equation of motion. The leg's inertia moment, however, make a little difference. The CoM positions are at the same as that of the active joint. The leg length or the radius of the RW is l [m]. The relative angle between two adjacent leg frames is $\alpha(=\pi/4)$ [rad].

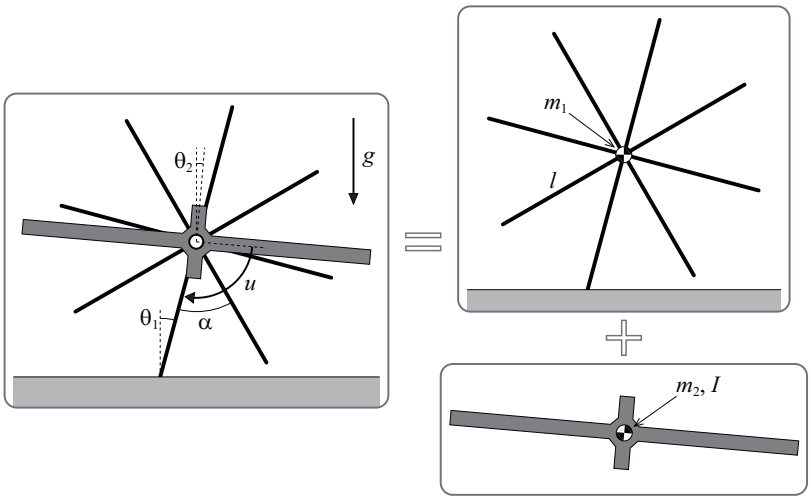

Fig. 1 Model of underactuated rimless wheel with torso

In this paper, we assume that the URW always contacts with the ground at one point without sliding. Let $\boldsymbol{\theta} = \begin{bmatrix} \theta_1 & \theta_2 \end{bmatrix}^{\mathrm{T}}$ be the generalized coordinate vector. Here, θ_1 is the angular position of the RW in the vertical direction, and θ_2 is that of the torso in the horizontal direction. The clockwise direction is set to the positive direction of rotation. The equation of motion during the single-support phase then becomes

$$\begin{bmatrix} Ml^2 & 0 \\ 0 & I \end{bmatrix} \begin{bmatrix} \ddot{\theta}_1 \\ \ddot{\theta}_2 \end{bmatrix} + \begin{bmatrix} -Mgl\sin\theta_1 \\ 0 \end{bmatrix} = \begin{bmatrix} 1 \\ -1 \end{bmatrix} u, \tag{1}$$

where $M := m_1 + m_2$ [kg] is the total mass of the URW. We denote Eq. (1) as

$$\boldsymbol{M}\ddot{\boldsymbol{\theta}} + \boldsymbol{g}\left(\boldsymbol{\theta}\right) = \boldsymbol{S}u. \tag{2}$$

As previously mentioned, the unilateral constraint condition (C3) must be also satisfied during motion as well as the stability of HZD. The vertical ground reaction force, F_z [N], can be determined as

$$F_z = M\left(g - l\ddot{\theta}_1\sin\theta_1 - l\dot{\theta}_1^2\cos\theta_1\right). \tag{3}$$

We then consider that a stable walking gait has been successfully generated only if F_z is always positive during motion. By considering

$$\ddot{\theta}_1 = \frac{u + Mgl\sin\theta_1}{Ml^2}, \tag{4}$$

Eq. (3) can be arranged to the following form without including angular accelerations.

$$F_z = M\cos\theta_1\left(g\cos\theta_1 - l\dot{\theta}_1^2\right) - \frac{u\sin\theta_1}{l} \tag{5}$$

2.2 Collision equations

Next, we outline the collision dynamics. As described later, the URW always achieves the constraint on impact posture, that is, it always falls down as a 1-DOF rigid body while maintaining $\dot{\theta}_1 = \dot{\theta}_2$ immediately before the next impact. In addition, we assume that the torso is mechanically locked to the RW during the collision (double-support) phase. This velocity constraint condition is mathematically represented by $\dot{\theta}_1^+ = \dot{\theta}_2^+$. On these assumptions, the transition equation for the angular velocity at impact becomes

$$\dot{\theta}_1^+ = \dot{\theta}_2^+ = \frac{Ml^2\cos\alpha + I}{Ml^2 + I}\dot{\theta}_1^-. \tag{6}$$

Under this condition, a strict output following control can be achieved as described later. On the other hand, in a steady gait the following relation holds.

$$\dot{\theta}_{1\mathrm{eq}}^+ = \dot{\theta}_{2\mathrm{eq}}^+ = \bar{R}\dot{\theta}_{1\mathrm{eq}}^-, \quad \bar{R} := \frac{Ml^2\cos\alpha + I}{Ml^2 + I} \tag{7}$$

Note that the subscript "eq" means the equilibrium on the Poincaré section, that is, the steady state at the collision phase. By subtracting Eq. (7) from Eq. (6), we get

$$\Delta\dot{\theta}_1^+ = \bar{R}\Delta\dot{\theta}_1^-, \quad \Delta\dot{\theta}_1^\pm := \dot{\theta}_1^\pm - \dot{\theta}_{1\mathrm{eq}}^\pm. \tag{8}$$

Therefore $\bar{R}$ is found to be the transition function of the state error for the collision phase, and we can understand that this phase is stable in terms of reduction of state error norm because $\left|\bar{R}\right| < 1$ holds [8,9].

3 Control design

3.1 Input-output linearization

Let

$$y := \boldsymbol{S}^{\mathrm{T}}\boldsymbol{\theta} = \theta_1 - \theta_2 \tag{9}$$

be the control output. The first- and second-order derivatives of y with respect to time then become

$$\frac{\mathrm{d}y}{\mathrm{d}t} = \frac{\partial y}{\partial \theta_1}\frac{\mathrm{d}\theta_1}{\mathrm{d}t}, \tag{10}$$

$$\frac{\mathrm{d}^2 y}{\mathrm{d}t^2} = \frac{\partial^2 y}{\partial \theta_1^2}\left(\frac{\mathrm{d}\theta_1}{\mathrm{d}t}\right)^2 + \frac{\partial y}{\partial \theta_1}\frac{\mathrm{d}^2\theta_1}{\mathrm{d}t^2}. \tag{11}$$

In the following, we denote the first- and second-order derivatives of y with respect to θ_1 as y' and y'' respectively. Eq. (11) is then expressed as

$$\ddot{y} = y''\dot{\theta}_1^2 + y'\ddot{\theta}_1. \tag{12}$$

Eq. (12) can be arranged to

$$y''\dot{\theta}_1^2 = \ddot{y} - y'\ddot{\theta}_1 = \bar{\boldsymbol{S}}^{\mathrm{T}}\ddot{\boldsymbol{\theta}}, \tag{13}$$

where

$$\bar{\boldsymbol{S}} := \begin{bmatrix} 1 - y' \\ -1 \end{bmatrix}. \tag{14}$$

y'' then becomes

$$y'' = \dot{\theta}_1^{-2}\bar{\boldsymbol{S}}^{\mathrm{T}}\ddot{\boldsymbol{\theta}} = \dot{\theta}_1^{-2}\bar{\boldsymbol{S}}^{\mathrm{T}}\boldsymbol{M}^{-1}\left(\boldsymbol{S}u - \boldsymbol{g}\left(\boldsymbol{\theta}\right)\right). \tag{15}$$

We can determine the control input, u, for achieving $y'' = v$ as:

$$u = \varGamma_1\left(\dot{\boldsymbol{\theta}}\right)^{-1}\left(v + \varGamma_2\left(\boldsymbol{\theta}, \dot{\boldsymbol{\theta}}\right)\right), \tag{16}$$

where

$$\varGamma_1\left(\dot{\boldsymbol{\theta}}\right) := \dot{\theta}_1^{-2}\bar{\boldsymbol{S}}^{\mathrm{T}}\boldsymbol{M}^{-1}\boldsymbol{S}, \quad \varGamma_2\left(\boldsymbol{\theta}, \dot{\boldsymbol{\theta}}\right) := \dot{\theta}_1^{-2}\bar{\boldsymbol{S}}^{\mathrm{T}}\boldsymbol{M}^{-1}\boldsymbol{g}\left(\boldsymbol{\theta}\right). \tag{17}$$

The state-space realization of $y'' = v$ becomes

$$\boldsymbol{x}' = \boldsymbol{A}\boldsymbol{x} + \boldsymbol{B}v, \tag{18}$$

where

$$\boldsymbol{x} = \begin{bmatrix} y \\ y' \end{bmatrix}, \quad \boldsymbol{A} = \begin{bmatrix} 0 & 1 \\ 0 & 0 \end{bmatrix}, \quad \boldsymbol{B} = \begin{bmatrix} 0 \\ 1 \end{bmatrix}.$$

3.2 Design of v and output trajectory

As previously mentioned, in this paper we propose a novel method to surely control y' to zero by the next impact or achieve the constraint on impact posture during the single-support phase with the assumption that the hip-joint is mechanically locked at impact. Then the derivative of the control output with respect to θ_1 should satisfy

$$(y')^{\pm} = \frac{\dot{y}^{\pm}}{\dot{\theta}_1^{\pm}} = \frac{\dot{\theta}_1^{\pm} - \dot{\theta}_2^{\pm}}{\dot{\theta}_1^{\pm}} = 0. \tag{19}$$

Since $\dot{\theta}_1^{\pm} > 0$ holds, Eq. (19) is equivalent to $\dot{y}^{\pm} = 0$.

We then design the control input, v, in the linear time-invariant (LTI) system of Eq. (18) to move $\boldsymbol{x}$ from an initial state:

$$\boldsymbol{x}_s := \boldsymbol{x}(\theta_s) = \begin{bmatrix} y_s \\ 0 \end{bmatrix} \tag{20}$$

to a terminal one:

$$\boldsymbol{x}_e := \boldsymbol{x}(\theta_e) = \begin{bmatrix} y_e \\ 0 \end{bmatrix}. \tag{21}$$

Note, however, that θ_s is the starting virtual-time of the output-following control, and θ_e is the ending virtual-time of it. Therefore they should satisfy the magnitude relation $\theta_e > \theta_s$.

In the following, we design a controller that keeps the control output y an initial constant value of y_s for $\theta_1^+ \leq \theta_1 < \theta_s$ and a terminal constant value of y_e for $\theta_e \leq \theta_1 < \theta_1^-$, and smoothly moves y from y_s to y_e during the period between θ_s and θ_e.

Since the LTI system (18) is controllable, we can consider the following control input.

$$v(\theta_1) = \boldsymbol{B}^{\mathrm{T}} \mathrm{e}^{-\boldsymbol{A}^{\mathrm{T}}\theta_1} \boldsymbol{G}\left(\theta_s, \theta_e\right)^{-1} \left(\mathrm{e}^{-\boldsymbol{A}\theta_e}\boldsymbol{x}_e - \mathrm{e}^{-\boldsymbol{A}\theta_s}\boldsymbol{x}_s\right) \tag{22}$$

Here, $\boldsymbol{G}\left(\theta_s, \theta_e\right)$ is a controllability grammian defined as

$$\boldsymbol{G}(\theta_s, \theta_e) := \int_{\theta_s}^{\theta_e} \mathrm{e}^{-\boldsymbol{A}\theta_1} \boldsymbol{B}\boldsymbol{B}^{\mathrm{T}} \mathrm{e}^{-\boldsymbol{A}^{\mathrm{T}}\theta_1} \mathrm{d}\theta_1 = \begin{bmatrix} \frac{1}{3}\left(\theta_e^3 - \theta_s^3\right) & -\frac{1}{2}\left(\theta_e^2 - \theta_s^2\right) \\ -\frac{1}{2}\left(\theta_e^2 - \theta_s^2\right) & \theta_e - \theta_s \end{bmatrix}. \tag{23}$$

The $v(\theta_1)$ of Eq. (22) is also detailed as

$$v(\theta_1) = -\frac{6(2\theta_1 - \theta_e - \theta_s)(y_e - y_s)}{(\theta_e - \theta_s)^3}. \tag{24}$$

This is a linear function of θ_1. Where $\theta_1 < \theta_s$ or $\theta_1 > \theta_e$, however, the control output must be kept constant. This is achieved by $y'' = 0$, and finally the $v(\theta_1)$ during the single-support phase is then specified as follows.

$$v(\theta_1) = \begin{cases} 0 & (\theta_1 < \theta_s) \\ -\dfrac{6(2\theta_1 - \theta_e - \theta_s)(y_e - y_s)}{(\theta_e - \theta_s)^3} & (\theta_s \le \theta_1 < \theta_e) \\ 0 & (\theta_1 \ge \theta_e) \end{cases} \tag{25}$$

By substituting Eq. (22) into Eq. (18) and solving it, the state vector $\boldsymbol{x}(\theta_1)$ for $\theta_s \le \theta_1 < \theta_e$ can be obtained as

$$\boldsymbol{x}(\theta_1) = \mathrm{e}^{\boldsymbol{A}\theta_1}\boldsymbol{x}_s + \int_{\theta_s}^{\theta_1} \mathrm{e}^{\boldsymbol{A}(\theta_1 - s)}\boldsymbol{B}v(s)\mathrm{d}s. \tag{26}$$

The first element, $y(\theta_1)$, and the second element, $y'(\theta_1)$, of $\boldsymbol{x}(\theta_1)$ are respectively detailed as follows.

$$y(\theta_1) = y_s - \frac{(\theta_1 - \theta_s)^2(2\theta_1 - 3\theta_e + \theta_s)(y_e - y_s)}{(\theta_e - \theta_s)^3} \tag{27}$$

$$y'(\theta_1) = -\frac{6(\theta_1 - \theta_e)(\theta_1 - \theta_s)(y_e - y_s)}{(\theta_e - \theta_s)^3} \tag{28}$$

The $y(\theta_1)$ draws a cubic curve in the configuration space of θ_1-y. The generated trajectory then consists of a cubic curve of Eq. (27) and straight lines in the configuration space.

In this paper, we start the output following control immediately after impact and set the boundary conditions as follows.

$$y_s = y^+ = -\frac{\alpha}{2}, \quad y_e = y^- = \frac{\alpha}{2}, \quad \theta_s = \theta_1^+ = -\frac{\alpha}{2} \tag{29}$$

Eqs. (25), (27) and (28) then become as follows.

$$v(\theta_1) = \begin{cases} -\dfrac{6\alpha\left(2\theta_1 - \theta_e + \frac{\alpha}{2}\right)}{\left(\theta_e + \frac{\alpha}{2}\right)^3} & \left(-\dfrac{\alpha}{2} \le \theta_1 < \theta_e\right) \\ 0 & (\theta_1 \ge \theta_e) \end{cases} \tag{30}$$

$$y(\theta_1) = \begin{cases} -\dfrac{\alpha}{2} - \dfrac{\alpha\left(\theta_1 + \frac{\alpha}{2}\right)^2\left(2\theta_1 - 3\theta_e - \frac{\alpha}{2}\right)}{\left(\theta_e + \frac{\alpha}{2}\right)^3} & \left(-\dfrac{\alpha}{2} \le \theta_1 < \theta_e\right) \\ \dfrac{\alpha}{2} & \left(\theta_e \le \theta_1 \le \dfrac{\alpha}{2}\right) \end{cases} \tag{31}$$

$$y'(\theta_1) = \begin{cases} -\dfrac{6\alpha(\theta_1 - \theta_e)\left(\theta_1 + \frac{\alpha}{2}\right)}{\left(\theta_e + \frac{\alpha}{2}\right)^3} & \left(-\dfrac{\alpha}{2} \le \theta_1 < \theta_e\right) \\ 0 & \left(\theta_e \le \theta_1 \le \dfrac{\alpha}{2}\right) \end{cases} \tag{32}$$

These are time-independent and change shape only according to θ_e. The $y(\theta_1)$ of Eq. (27) is a natural solution in terms of the control of a LTI system. The control input $v(\theta_1)$ for it, however, is not continuous at $\theta_1 = \theta_e$. The left-hand limit of $v(\theta_1)$ where $\theta_1 = \theta_e$ becomes

$$v(\theta_e^-) = \lim_{\theta_1 \nearrow \theta_e} v(\theta_1) = \lim_{\theta_1 \nearrow \theta_e} \frac{-6\alpha\left(2\theta_1 - \theta_e + \frac{\alpha}{2}\right)}{\left(\theta_e + \frac{\alpha}{2}\right)^3} = -\frac{6\alpha}{\left(\theta_e + \frac{\alpha}{2}\right)^2}, \tag{33}$$

whereas the right-hand limit becomes

$$v(\theta_e^+) = \lim_{\theta_1 \searrow \theta_e} v(\theta_1) = 0. \tag{34}$$

From the above results, it is shown that $v(\theta_e^+) \neq v(\theta_e^-)$ holds for all $\alpha > 0$.

The generated trajectory of the control output, $y(\theta_1)$, is a cubic function of θ_1 as mentioned. To make $v(\theta_1)$ continuous at $\theta_1 = \theta_e$, we must specify $y(\theta_1)$ as a polynomial function of θ_1 that is at least fifth-order [8,9]. Investigation of the gait properties with higher-order $y(\theta_1)$ is an issue in the future.

Figure 2 plots the trajectories of (a) the $v(\theta_1)$ of Eq. (30), (b) the $y(\theta_1)$ of Eq. (31), and (c) the $y'(\theta_1)$ of Eq. (32) where $\theta_s = -\alpha/2 = -\pi/8$ and $\theta_e = 0.15$ [rad]. To clearly show their properties, we also plotted the lines of $\theta_1 = \pm\pi/8$, $\theta_1 = 0.15$, and zero lines. We can see that, for $\theta_s \leq \theta_1 \leq \theta_e$, the $v(\theta_1)$ draws a straight line, $y(\theta_1)$ draws a cubic curve, and $y'(\theta)$ draws a quadratic curve according to the equations. These are independent of the robot's physical parameters and does not change their shapes unless the boundary conditions are modified. The relationship between the shape of $y(\theta_1)$ (gait symmetry) and restored mechanical energy (gait properties) will be discussed in the next section.

3.3 Singularity and continuity of control input

Note that $\mathit{\Gamma}_1\left(\dot{\boldsymbol{\theta}}\right)$ and $\mathit{\Gamma}_2\left(\boldsymbol{\theta}, \dot{\boldsymbol{\theta}}\right)$ of Eq. (17) have a singularity at $\dot{\theta}_1 = 0$, but it does not matter for the following reason. The control input becomes

$$\begin{aligned} u &= \frac{v(\theta_1)}{\mathit{\Gamma}_1\left(\dot{\boldsymbol{\theta}}\right)} + \frac{\mathit{\Gamma}_2\left(\boldsymbol{\theta}, \dot{\boldsymbol{\theta}}\right)}{\mathit{\Gamma}_1\left(\dot{\boldsymbol{\theta}}\right)} \\ &= \frac{\dot{\theta}_1^2 v(\theta_1)}{\bar{\boldsymbol{S}}^{\mathrm{T}} \boldsymbol{M}^{-1} \boldsymbol{S}} + \frac{\bar{\boldsymbol{S}}^{\mathrm{T}} \boldsymbol{M}^{-1} \boldsymbol{g}(\boldsymbol{\theta})}{\bar{\boldsymbol{S}}^{\mathrm{T}} \boldsymbol{M}^{-1} \boldsymbol{S}} \\ &= \frac{Ml^2 I \dot{\theta}_1^3 v(\theta_1)}{L} - \frac{MglI\dot{\theta}_2 \sin\theta_1}{L}, \end{aligned} \tag{35}$$

where

$$L := Ml^2\dot{\theta}_1 + I\dot{\theta}_2 \tag{36}$$

is the angular momentum about the contact point. Therefore the control input can be determined unless L vanishes.

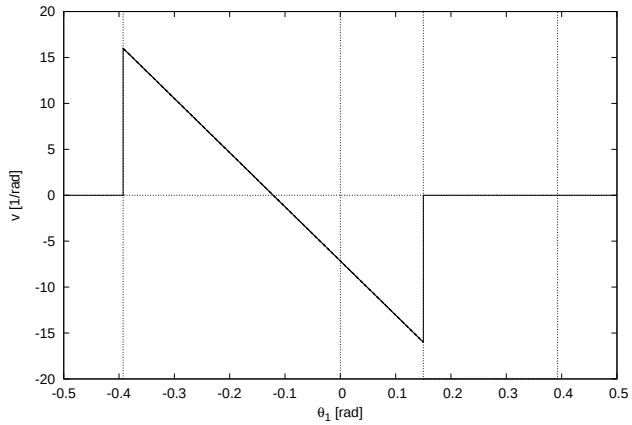

(a) v versus θ_1

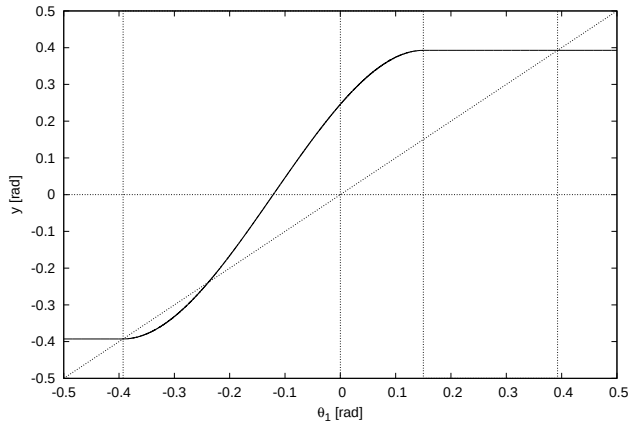

(b) y versus θ_1

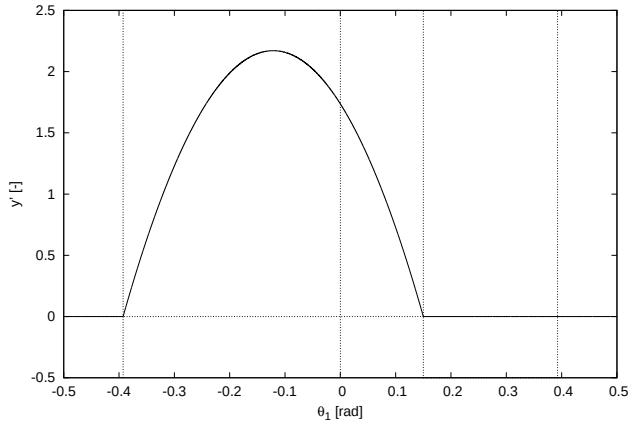

(c) y' versus θ_1

Fig. 2 v, y, and y' versus θ_1

4 Gait analysis

4.1 Relationship between gait symmetry and mechanical energy restoration

First, we conduct numerical simulations to observe the typical walking gaits and how the gait properties change according to the gait symmetry. We set the physical parameters to the values listed in Table 1.

Figure 3 shows the simulation results of dynamic walking where $\theta_e = \alpha/2 = \pi/8$ [rad]. Here, (a) is the angular positions, (b) the angular velocities, and (c) the mechanical energy. The physical parameters of the URW are chosen as listed in Table 1. Figure 4 shows the generated trajectory in the configuration space of θ_1–y. We can see that the generated trajectory is symmetric about the coordinate origin of the configuration space as in [5–7], and that the URW falls backward because it cannot overcome the potential barrier at mid-stance. This is because the URW has the simplest shape of a single inverted pendulum, and it generates time-symmetric trajectories of mechanical energy during the single-support phases. If the URW does not have the simplest shape, the trajectory of mechanical energy becomes time-asymmetric and a stable walking gait can be generated with suitable physical and initial parameters. In Passive Velocity Field Control (PVFC) [11,12] the contour following speed is controlled according to the external energy sources, whereas our method controls it according to the body shape or frame asymmetry. In other words, we can achieve mechanical energy restoration by modifying the shape of the body frame instead of changing the desired output trajectory or control equation.

In this paper, however, we mainly discuss the relationship between the gait symmetry in the configuration space and mechanical energy restoration without changing the simplest body shape. We then adjust θ_e and investigate how the generated gait property changes according to the gait symmetry.

Figure 5 shows the simulation results of dynamic walking where $\theta_e = 0.20$ [rad]. Figure 6 shows the generated trajectory in the configuration space of θ_1–y. From Fig. 6, we can see that the generated trajectory is asymmetric about the coordinate origin of the configuration space, and that it consists of a part of a cubic curve and a straight line. Fig. 5 (c) shows that the mechanical energy is accordingly restored during the single-support phases. In this case, however, the gait asymmetry is not sufficient and the URW finally falls backward because overcoming the potential barrier at mid-stance becomes impossible.

Figure 7 shows the simulation results of dynamic walking where $\theta_e = 0.15$ [rad]. Figure 8 shows the generated trajectory in the configuration space of

Table 1 Physical parameters

m_1	1.0	kg
m_2	1.0	kg
I	1.0	kg·m^2
l	1.0	m
α	$\pi/4$	rad

θ_1–y. We can see that the generated trajectory is more asymmetric about the coordinate origin of the configuration space than the previous one, and that the mechanical energy is accordingly restored more than the previous case during the single-support phases. In this case, the gait asymmetry is sufficient and the walking motion converges to a stable limit cycle.

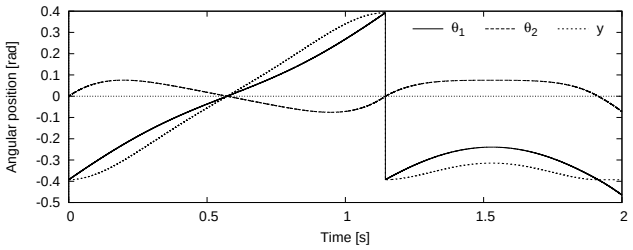

(a) Angular position

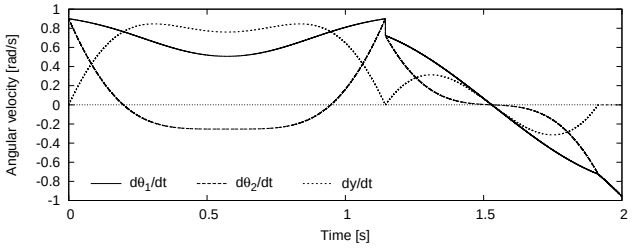

(b) Angular velocity

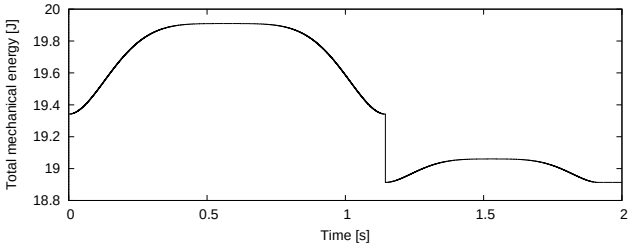

(c) Total mechanical energy

Fig. 3 Simulation results where $\theta_e = \pi/8$ [rad]

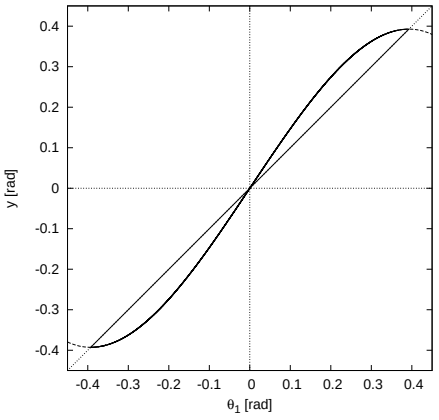

Fig. 4 Simulation result where $\theta_e = \pi/8$ [rad]

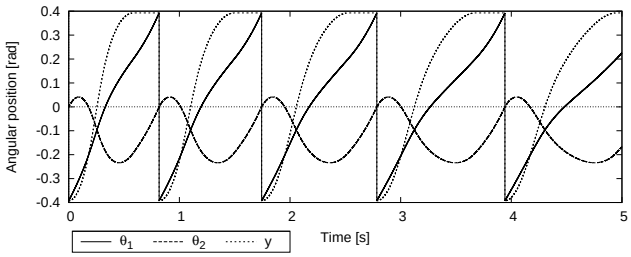

(a) Angular position

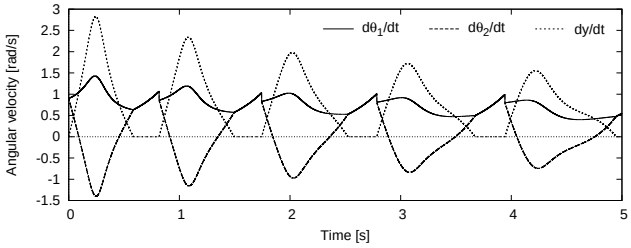

(b) Angular velocity

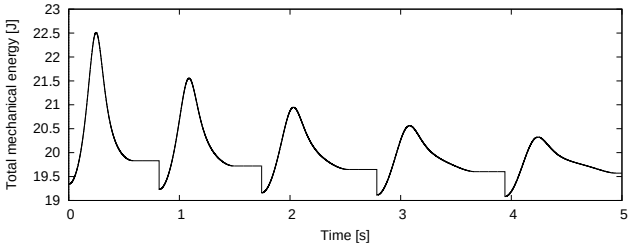

(c) Total mechanical energy

Fig. 5 Simulation results where $\theta_e = 0.20$ [rad]

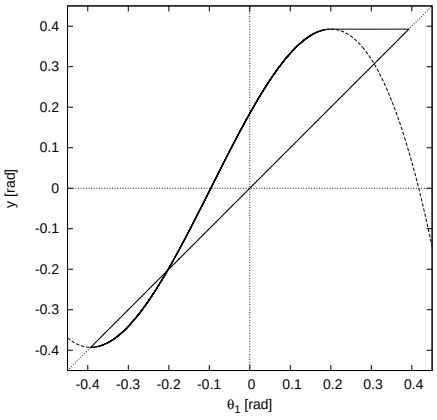

Fig. 6 Simulation result where $\theta_e = 0.20$ [rad]

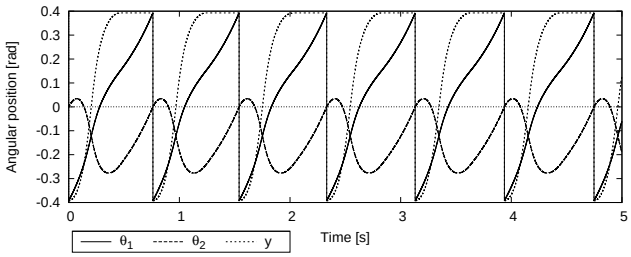

(a) Angular position

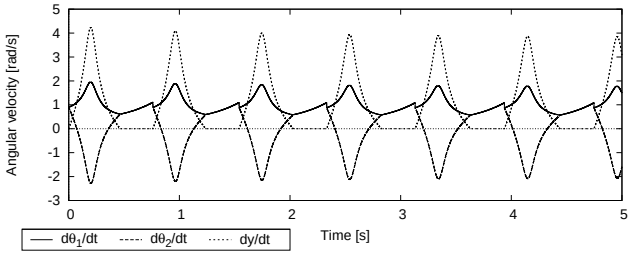

(b) Angular velocity

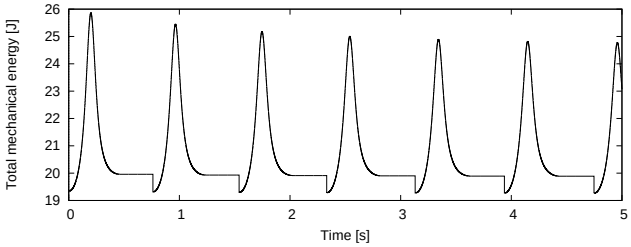

(c) Total mechanical energy

Fig. 7 Simulation results where $\theta_e = 0.15$ [rad]

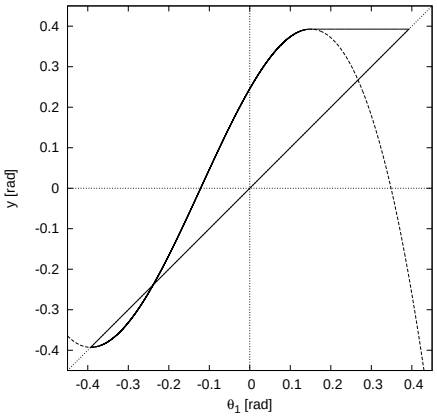

Fig. 8 Simulation result where $\theta_e = 0.15$ [rad]

4.2 Efficiency analysis

Before analysis, we define some criteria for gait efficiencies. Let T [s] be the steady step period. The walking speed, V [m/s], is then defined as

$$V := \frac{\Delta X_g}{T}, \tag{37}$$

where ΔX_g [m] is the travel distance of the CoM in one step, that is,

$$\Delta X_g := 2l \sin \frac{\alpha}{2}. \tag{38}$$

Since this is a constant, the walking speed varies in inverse proportion to T. The transfer efficiency of walking robots is commonly evaluated in terms of the specific resistance (SR) which is defined as

$$\mathrm{SR} := \frac{1}{Mg\Delta X_g} \int_{0^+}^{T^-} |\dot{y}u| \, \mathrm{d}t = \frac{1}{Mg\Delta X_g} \int_{0^+}^{T_e^-} \dot{y} \, |u| \, \mathrm{d}t, \tag{39}$$

where T_e [s] is the instant of time when θ_1 reaches θ_e. The second equality holds because

$$\dot{y} = y'(\theta_1)\dot{\theta}_1 = -\frac{6\alpha(\theta_1 - \theta_e)\left(\theta_1 + \frac{\alpha}{2}\right)}{\left(\theta_e + \frac{\alpha}{2}\right)^3}\dot{\theta}_1 \tag{40}$$

and $y'(\theta_1)$ is a parabola convex upward. Therefore $\dot{y}$ is non-negative for $\theta_s = -\alpha/2 \leq \theta_1 \leq \theta_e$ if $\dot{\theta}_1 \geq 0$. The SR implies the expenditure of energy per unit mass and per unit travel distance. The SR is therefore small means the generated gait is energy efficient.

Figure 9 plots the gait descriptors with respect to θ_e. The physical parameters are chosen as the same in the previous subsection. Here, (a) is the step period, (b) the walking speed, (c) the specific resistance, and (d) the restored mechanical energy. It seems that the restored mechanical energy, (d), varies in proportion to θ_e. The gait descriptors are plotted at intervals of $\theta_e = 0.001$ [rad]. From Fig. 9 (d), we can see that the restored mechanical energy monotonically decreases as θ_e increases. This is because the generated gait is symmetrized as θ_e approaches $-\theta_s$, and the restored mechanical energy accordingly decreases to zero. Figs. 9 (a) and (b) imply that the reduction of the restored mechanical energy makes overcoming potential barrier at mid-stance more difficult. On the other hand, stable gait generation becomes impossible as θ_e decreases. This is because the unilateral constraint condition cannot be met or the ground reaction force F_z determined by Eqs. (3) or (5) becomes negative during the single-support phase due to excessive input torque caused by the fast control.

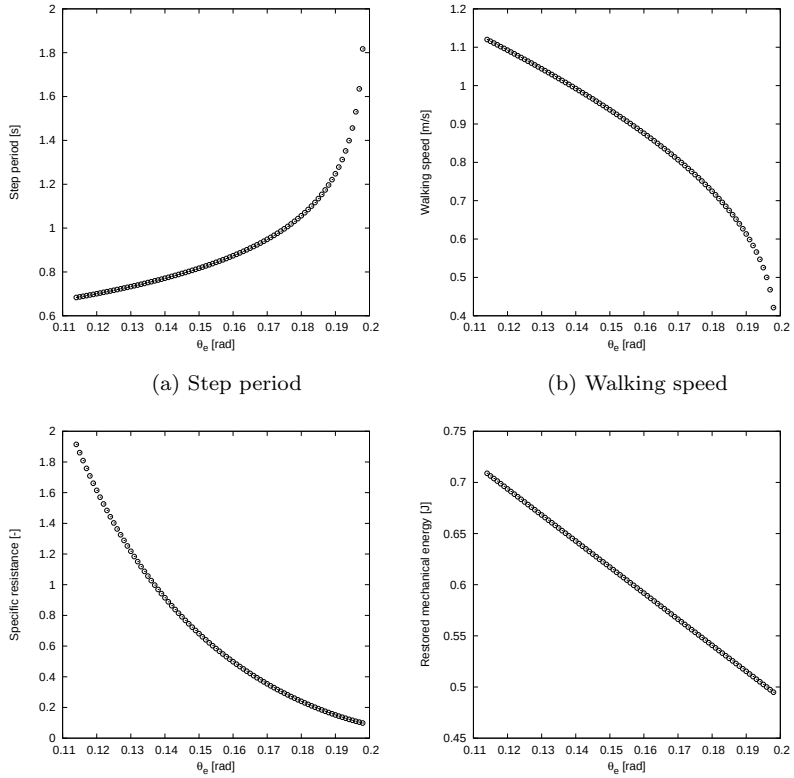

(a) Step period (b) Walking speed

(c) Specific resistance (d) Restored mechanical energy

Fig. 9 Gait descriptors versus θ_e

4.3 Restored mechanical energy and asymptotic stability

In this subsection, we mathematically show that the restored mechanical energy becomes constant according to the proposed method.

The total mechanical energy, E, is given by

$$E = \frac{1}{2}\dot{\boldsymbol{\theta}}^{\mathrm{T}}\boldsymbol{M}\dot{\boldsymbol{\theta}} + P(\boldsymbol{\theta}), \tag{41}$$

where $P(\boldsymbol{\theta}) := Mgl\cos\theta_1$ is the potential energy. The time derivative of E satisfies

$$\dot{E} = \dot{\boldsymbol{\theta}}^{\mathrm{T}}\boldsymbol{S}u = \dot{y}u. \tag{42}$$

The restored mechanical energy in the (i)th step, ΔE_i, then becomes

$$\Delta E_i = \int_{0^+}^{T_i^-} \dot{y}u\mathrm{d}t = \int_{0^+}^{T_e^-} \dot{y}u\mathrm{d}t. \tag{43}$$

Following Eq. (9), the second-order derivative of y with respect to time becomes

$$\ddot{y} = \boldsymbol{S}^{\mathrm{T}}\ddot{\boldsymbol{\theta}} = \boldsymbol{S}^{\mathrm{T}}\boldsymbol{M}^{-1}\left(\boldsymbol{S}u - \boldsymbol{g}(\boldsymbol{\theta})\right). \tag{44}$$

By multiplying both sides of Eq. (44) by $\dot{y}$, we get

$$\dot{y}\ddot{y} = \left(\boldsymbol{S}^{\mathrm{T}}\boldsymbol{M}^{-1}\boldsymbol{S}u - \boldsymbol{S}^{\mathrm{T}}\boldsymbol{M}^{-1}\boldsymbol{g}(\boldsymbol{\theta})\right)\dot{y}. \tag{45}$$

The time integral of the left-hand side of Eq. (45) for the (i)th step becomes

$$\int_{0^+}^{T_e^-} \dot{y}\ddot{y}\mathrm{d}t = \left[\frac{\dot{y}^2}{2}\right]_{0^+}^{T_e^-} = \left[\frac{\left(y'(\theta_1)\dot{\theta}_1\right)^2}{2}\right]_{0^+}^{T_e^-} = 0. \tag{46}$$

Therefore, the time integral of the right-hand side of Eq. (45) for the (i)th step becomes

$$\int_{0^+}^{T_e^-} \left(\boldsymbol{S}^{\mathrm{T}}\boldsymbol{M}^{-1}\boldsymbol{S}u - \boldsymbol{S}^{\mathrm{T}}\boldsymbol{M}^{-1}\boldsymbol{g}(\boldsymbol{\theta})\right)\dot{y}\mathrm{d}t = 0, \tag{47}$$

and this is arranged to

$$\int_{0^+}^{T_e^-} \dot{y}u\mathrm{d}t = \int_{0^+}^{T_e^-} \frac{\boldsymbol{S}^{\mathrm{T}}\boldsymbol{M}^{-1}\boldsymbol{g}(\boldsymbol{\theta})}{\boldsymbol{S}^{\mathrm{T}}\boldsymbol{M}^{-1}\boldsymbol{S}}\dot{y}\mathrm{d}t = -\int_{0^+}^{T_e^-} \frac{MglI\sin\theta_1}{Ml^2+I}\dot{y}\mathrm{d}t \tag{48}$$

By considering $\dot{y} = y'(\theta_1)\dot{\theta}_1$, we can arrange Eq. (48) to

$$\begin{aligned}
\int_{0^+}^{T_e^-} \dot{y}u\mathrm{d}t &= -\int_{-\alpha/2}^{\theta_e} \frac{MglI\sin\theta_1}{Ml^2+I}y'(\theta_1)\mathrm{d}\theta_1 \\
&= \frac{6\alpha MglI}{(Ml^2+I)\left(\theta_e+\frac{\alpha}{2}\right)^3}\int_{-\alpha/2}^{\theta_e}(\theta_1-\theta_e)\left(\theta_1+\frac{\alpha}{2}\right)\sin\theta_1\mathrm{d}\theta_1 \\
&= \frac{6\alpha MglI}{(Ml^2+I)\left(\theta_e+\frac{\alpha}{2}\right)^3} \\
&\quad\times\left(2\left(\cos\theta_e-\cos\frac{\alpha}{2}\right)+\left(\theta_e+\frac{\alpha}{2}\right)\left(\sin\theta_e-\sin\frac{\alpha}{2}\right)\right)
\end{aligned} \tag{49}$$

Therefore, we can conclude that the value of the restored mechanical energy of the (i)th step, ΔE_i, is constant and is changed only according to θ_e.

Figure 10 plots the numerical restored mechanical energy for five values of the inertia moment, I, with respect to θ_e. The numerical results are dotted at intervals of $\theta_e = 0.002$ [rad]. The analytical solution for each I given by Eq. (49) is represented with a dotted line. All the dotted lines intersect at $\theta_e = -\theta_s$ where $\Delta E_i = 0$ holds. We can see that the numerical result is coincides with the analytical solution in each case. As is the case in Fig. 9, in all cases overcoming the potential barrier becomes impossible as θ_e increases and the ground reaction force becomes negative as θ_e decreases.

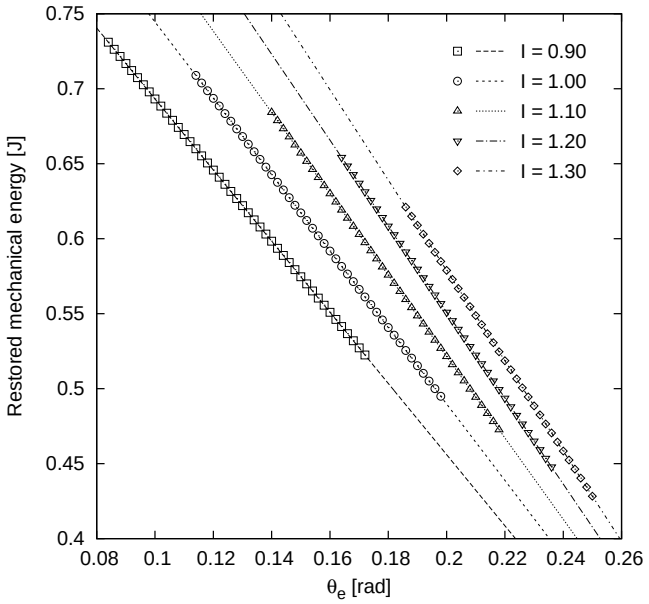

Fig. 10 Numerical results and their analytical solutions of restored mechanical energy for five values of I

In the following, ΔE denotes the constant restored mechanical energy given by Eq. (49). Since the constraint on impact posture is achieved, the energy-loss coefficient, $\varepsilon = \bar{R}^2$, becomes constant and the following recurrence formula holds [9].

$$K_{i+1}^{-} = \varepsilon K_i^{-} + \Delta E \tag{50}$$

Where K_i^{-} is the kinetic energy immediately before the (i)th impact. Since both ε and ΔE are constants, the limit value of K_i^{-} becomes

$$\lim_{i\to\infty} K_i^{-} = \frac{\Delta E}{1-\varepsilon}. \tag{51}$$

This is a proof of the asymptotic stability of the generated walking gait or the HZD [9].

Note that we could solve Eq. (47) for the integral from 0^{+} to T_e of $\dot{y}u$ because the term

$$\boldsymbol{S}^{\mathrm{T}}\boldsymbol{M}^{-1}\boldsymbol{S} = \frac{Ml^2 + I}{Ml^2 I} \tag{52}$$

is a constant. This is a unique nature of the URW. In general biped robots, however, the inertia matrix is not constant and we must consider an approximate solution.

Figure 11 shows the evolution of the gait descriptors for three values of I with respect to the step number where $\theta_e = 0.15$ [rad]. In this case, as indicated in Fig. 10, stable walking gaits could not be generated for $I = 0.120$

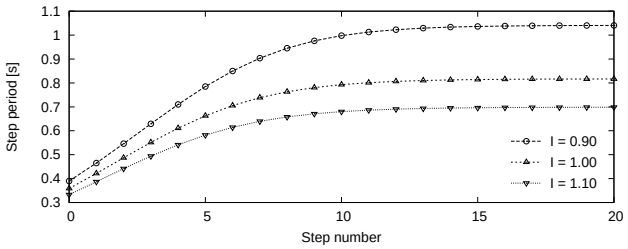

(a) Step period

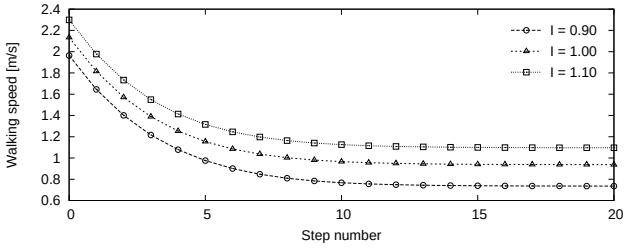

(b) Walking speed

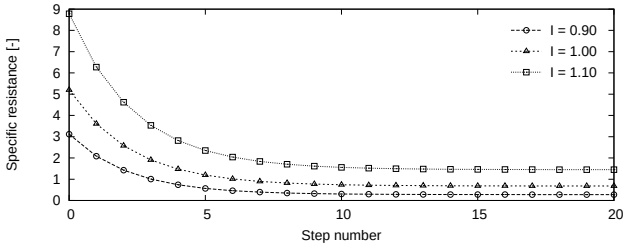

(c) Specific resistance

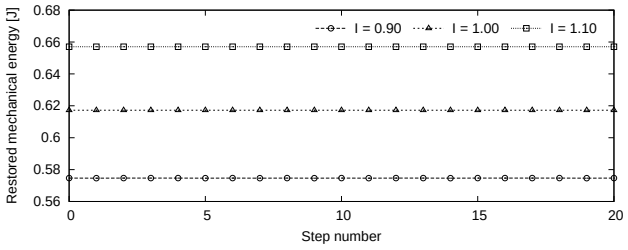

(d) Restored mechanical energy

Fig. 11 Evolution of gait descriptors for three values of I where $\theta_e = 0.15$ [rad]

and 0.130 [kg·m^2] because the unilateral constraint condition could not be satisfied. As indicated in Figs. 9 and 10, asymptotically stable gait generation can be achieved with various θ_e and the robot's physical parameters such as I. We must numerically determine, however, if the setting value of θ_e is valid for the physical parameters and vice versa. Here, (a) is the step period, (b) the walking speed, (c) the specific resistance, and (d) the restored mechanical

energy. In these figures, we defined the gait descriptors with each step as follows. Let T_i [s] be the step period of (i)th step. The walking speed for the (i)th step is then defined as

$$V_i := \frac{\Delta X_g}{T_i}, \tag{53}$$

where ΔX_g is the same as Eq. (38) and is constant. The SR for the (i)th step is also defined as

$$\mathrm{SR}_{(i)} := \frac{1}{Mg\Delta X_g}\int_{0^+}^{T_i^-} |\dot{y}u|\,\mathrm{d}t = \frac{1}{Mg\Delta X_g}\int_{0^+}^{T_e^-} \dot{y}\,|u|\,\mathrm{d}t. \tag{54}$$

From Fig. 11, we can see that the walking motion monotonically converges to a limit cycle in all cases, that is, the generated gait is asymptotically stable. Fig. 11 (d) strongly supports that the restored mechanical energy is kept constant in all cases.

5 Conclusion and future work

In this paper, we proposed a novel method for generating an asymptotically-stable walking gait that ensures the achievement of the constraint on impact posture. We numerically investigated the fundamental gait properties and mathematically proved that the generated gait is always asymptotic stability because the constraint on restored mechanical energy is simultaneously achieved.

The proposed method can be applied to general mechanical systems that generate the steady motion as a limit cycle with state jumps. The hybrid zero dynamics, however, must be inherently stable and must monotonically increase or decrease with respect to time. Limit cycle walking is the best example of the application. In the URW model, it is mathematically possible to generate an asymptotically-stable walking gait according to our method unless it cannot overcome the potential barrier at mid-stance. As mentioned, this is because the inertia matrix of the URW model or the term $\boldsymbol{S}^{\mathrm{T}}\boldsymbol{M}^{-1}\boldsymbol{S}$ are constant. In different models with variable inertia matrix, however, the same can be also expected under the condition that the nonlinearity of the model is not so high. The inertia matrix of the simple biped models also becomes constant by linearization [8,9]. The validation of stability analysis based on linearization is a subject of future investigation. Further investigation taking the condition for overcoming potential barrier into account is also left as a future work.

Acknowledgements This research was partially supported by a Grant-in-Aid for Scientific Research, (C) No. 24560542, provided by the Japan Society for the Promotion of Science (JSPS).

References

1. McGeer, T.: Passive dynamic walking, Int. J. of Robotics Research, Vol. 9, No. 2, pp. 62–82 (1990)
2. McGeer, T.: Passive walking with knees, Proc. of the IEEE Int. Conf. on Robotics and Automation, Vol. 3, pp. 1640–1645 (1990)
3. Coleman, M. J., Chatterjee, A., Ruina, A.: Motions of a rimless spoked wheel: a simple three-dimensional system with impacts, Dynamics and Stability of Systems, Vol. 12, Iss. 3, pp. 139–159 (1997)
4. Westervelt E. R., Grizzle, J.W., Chevallereau, C., Choi, J. H., Morris, B.: Feedback Control of Dynamic Bipedal Robot Locomotion, CRC Press (2007)
5. Morita, S. and Ohtsuka, T.: Gait generation method for a compass type walking machine using dynamical symmetry, Proc. of the IEEE/RSJ Int. Conf. on Intelligent Robots and Systems, pp. 2825–2830 (2004)
6. Hyon, S.-H. and Emura, T.: Symmetric walking control: Invariance and global stability, Proc. of the IEEE Int. Conf. on Robotics and Automation, pp. 1443–1450 (2005)
7. Asano, F. and Luo, Z.-W.: Efficiency and symmetry of ballistic gait, Proc. of the IEEE/RSJ Int. Conf. on Intelligent Robots and Systems, pp. 2928–2933 (2008)
8. Asano, F.: Stability analysis method independent of numerical integration for limit cycle walking with constraint on impact posture, Proc. of the IEEE Int. Conf. on Robotics and Automation, pp. 4647–4652 (2014)
9. Asano, F.: Fully analytical solution to discrete behavior of hybrid zero dynamics in limit cycle walking with constraint on impact posture, Multibody System Dynamics, published as an online first view article. doi:10.1007/s11044-014-9445-4
10. Vukobratović, M. and Stepanenko, J.: On the stability of anthropomorphic systems, Mathematical Biosciences, Vol. 15, pp. 1–37 (1972)
11. Li, P. Y. and Horowitz, R.: Passive velocity field control (PVFC): part I–geometry and robustness, IEEE Trans. on Automatic Control, Vol. 46, No. 9, pp. 1346–1359 (2001)
12. Li, P. Y. and Horowitz, R.: Passive velocity field control (PVFC): part II–application to contour following, IEEE Trans. on Automatic Control, Vol. 46, No. 9, pp. 1360–1371 (2001)